ChemComm

Accepted Manuscript

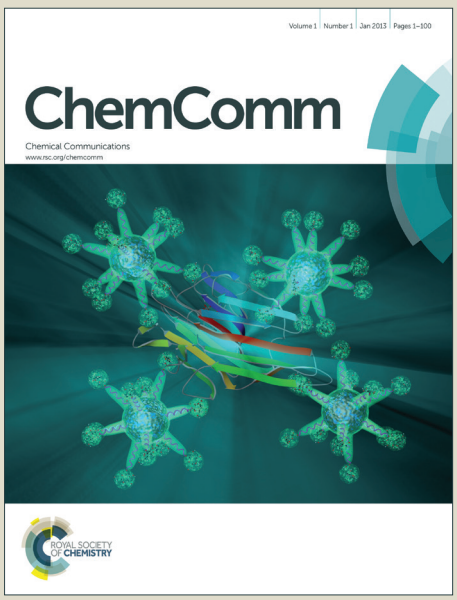

ROYAL SOCIETY OF CHEMISTRY

www.rsc.org/chemcomm

Cite this: DOI: 10.1039/c0xx00000x

www.rsc.org/xxxxxx

Modified deposition process of electron transport layer for efficient inverted planar perovskite solar cells

Hua Dong,[#a] Zhaoxin Wu,[#*a] Bin Xia,[a] Jun Xi,[a] Fang Yuan,[a] Shuya Ning,[a] Lixin Xiao,*[b] and Xun Hou[a]

Received (in XXX, XXX) Xth XXXXXXXXX 20XX, Accepted Xth XXXXXXXXX 20XX

DOI: 10.1039/b000000x

A high-efficient inverted heterojunction perovskite solar cell was demonstrated. Homogeneous and compact perovskite ($CH_3NH_3PbI_3$) layer was prepared via a two-step solution deposition method, subsequently a double-layer PCBM film was deposited by sequential spin-coating/vapor deposition process as the electron transport layer. The optimal device could achieve a 12.2% (average 11.09%) efficiency.

Hybrid organometal halide perovskite solar cells have received much attention due to their superior intrinsic properties for solar energy conversion. This type of solar cells was first reported by Miyasaka et, al with a power conversion efficiency (PCE) of 4%,[1] and despite going through only several years the efficiency soon evolved to over 19%.[2-5] The hybrid perovskite materials exhibit appealing features such as high absorption coefficient, excellent ambipolar charge mobility, and appropriate band gap.[6-8] Moreover, the simple cell configuration and low cost fabrication process of this solar cell could further address the scalability and application in Photovoltaic field.[9]

Recently, typical perovskite solar cells employed an electron-transport layer (ETL)/perovskite material/hole-transport layer (HTL) structure. Initial mesosuperstructure-type solar cells based on mesoporous-TiO_2 layer as electron-transport layers requires high-temperature processing (>450 °C), which hinders the commercialization.[10-12] Therefore, many approaches were developed to avoid high-temperature barrier. As one promising approach, planar-inverted heterojunction device architecture is particularly interesting due to the simple cell configuration and possible low-temperature fabrication.[8, 13] The use of phenyl-C61-butyric acid methyl ester (PCBM) as electron-transport layer has been investigated by several groups.[14, 15] However, perovskite films with incomplete and non-homogeneous coverage via one-step spin-coating was usually observed in planar perovskite solar cells, and these subsequent disadvantages have been regarded as the barrier resulting in decreased device performance. [16, 17]

Many efforts have been made to control the morphology of perovskite thin films. Various modified one-step spin-coating deposition methods were investigated such as adding DIO and GBL as the additive for achieving a high coverage perovskite layer.[17, 18] However, bareness and non-homogeneous problem can not still be completely avoided. Bolink et al proposed the evaporation sublimation method and achieved >12% efficiency of the solar cell.[4] Those work demonstrated the great potential of the perovskite–PCBM architecture. However, the complicated and rigorous fabrication process of the perovskite layer maybe constraint on the application, meanwhile the monitoring and control of the perovskite layer deposition by vacuum sublimition is difficult.[3, 4 19]

It is known that perovskite film based on two-step solution-process could promise the strong light-harvesting, good charge transport and complete coverage, which have been demonstrated in the high-temperature mesoporous devices.[18, 20] Whereas such a technology was rarely applied in planar perovskite–PCBM solar cell, and reported perovskite–PCBM device based on two-step only show a less 8% efficiency,[21, 22] It is mainly because that the two-step solution-processed perovskite layer is quite rough and the subsequent ETL hardly fill in the undulation and smooth the interface between ETL and metal electrode. As a relative easy-fabrication and low-temperature planar perovskite–PCBM solar cell, its more higher efficiency is quite desireable.

In this article, we developed a simple and effective method to enhance the performance of perovskite-PCBM solar cell based on two-step solution-processed perovskite layer, and the device configuration was shown in **Fig.1**(a). The structure is designed as: glass, ITO substrate, HTL PEDOT:PSS, $CH_3NH_3PbI_3$ ($MAPbI_3$), ETL PCBM (layer-by-layer) and Ag electrode.

As one type of fullerene derivative, PCBM was the most pervasive ETL applied in planar heterojunction perovskite solar cell. Considering the membranous and solubility of the material, reported thickness of the PCBM is located in dozens of nanometers by spin-coating. This range could satisfy the covering requirement of the solar cell based on one-step solution or vapor deposition technology to obtain the considerable efficiency.

However, the only spin-coating process could hardly fill in and cover the rough perovskite layer by two-step solution completely, which would lead to the charge recombination losses and influenced the transport at the interface. Here we designed a sequential solution-vapor deposition process for preparing PCBM

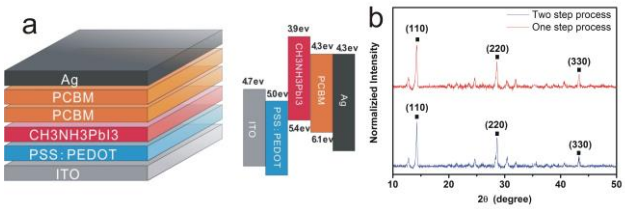

Fig. 1 (a) Device structure and energy band diagram of the perovskite–PCBM solar cell. (b) X-ray diffraction spectra of the one-step and two–step solution-processed perovskite ($CH_3NH_3PbI_3$) film.

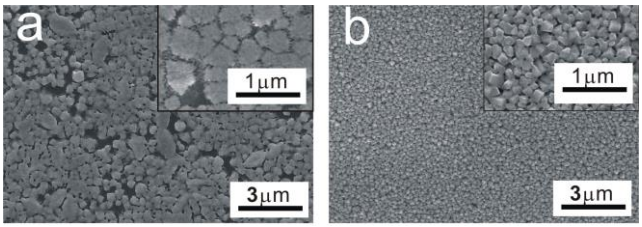

Fig. 3 SEM top views of the one-step (a) and two-step (b) solution-processed deposited perovskite films.

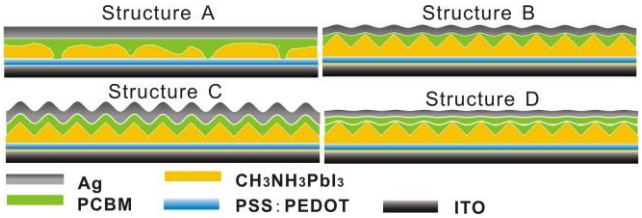

Fig. 4 the Schema of the four types of structures:
A: ITO/PEDOT/$MAPbI_3$(one-step)/PCBM(spin-coating)/Ag
B: ITO/PEDOT/$MAPbI_3$(two-step)/PCBM(spin-coating)/Ag
C: ITO/PEDOT/$MAPbI_3$(two-step)/PCBM(Vaporing)/Ag
D: ITO/PEDOT/$MAPbI_3$(two-step)/PCBM(spin-coating)/PCBM(vaporing)/Ag

layer, the highlight in our study, to solve this problem. The initial spin-coating process could fill in the depression of $MAPbI_3$ layer preliminary, then the sequential vapor deposition process could further smooth the interface and separate the $MAPbI_3$ layer and Ag electrode. Through optimizing the fabrication process, a finally PCBM layer with moderate thickness, good film property and the planar surface can be obtained. The solar cell based on the sequential PCBM layer can achieve a high light harvesting efficiency as well as good charge transport. The best device shows a 12.2% high efficiency with V_{oc}=0.99 V, J_{sc}=18.11 mA/cm^2, FF=0.68, and this efficiency is superior to that of the reported perovskite-PCBM devices based on two-step $MAPbI_3$ layer.[21, 22] We hope that as an easy-fabrication and high efficient structure, this modified solution-processed based perovskite solar cell could provide a new way for promoting the development of this hot solar cell.

In **Fig. 1**(b), we first compared the X-ray diffraction pattern of films of $CH_3NH_3PbI_3$ by either one-step or two-step deposition method, Strong peaks at 14.03° and 27.52° corresponding to the (110) and (220) planes confirm the formation of a tetragonal perovskite structure with lattice parameters.[3] There is only a small signature of a peak at 12.65° (the (001) diffraction peak for PbI_2). It indicated that the two $MAPbI_3$ films both present the high level of phase purity, and it was also the precondition of achieving the high efficient perovskite solar cells.

The top-view SEM images in **Fig. 3**a, b shows the differences between the $MAPbI_3$ film morphologies produced by the two deposition processes. It can be seen that $MAPbI_3$ film based on one-step has the low coverage and large voids. This shapeless perovskite morphology has been cited as very detrimental to the performance because it not only causes electrical shorting but also leads to the charge dissociation/transport/recombination.[23] Whereas the cube-like $MAPbI_3$ film with ~200 nm domain sizes based on two-step present the homogeneous and complete coverage on the substrate. It is known that a highly roughened interface would strengthen internal light scattering, and the larger crystallites and interface area also benefit the charge transport.[24] The properties have been demonstrated in reported mesoporous TiO_2-based perovskite solar cell, and we hope to develop these mentioned advantages in planar PCBM-perovskite solar cell.

As for the planar PVK solar cell, high PCE requires both strong light harvesting and good charge transport at the interfaces. So how to effictively fill in and smooth the rough perovskite layer is important, only then it could provide the good interface contact for charge-transporting as well as utilize the advantages of the two-step perovskite layer. The modified fabrication process of the PCBM layer is studied for achieving the win-win situation in our study. Here we designed devices with three PCBM deposition methods for developing the most appropriate deposition way: only spin-coating; only vaporing and sequential spin-vapor deposition. Device based on one-step $MAPbI_3$ layer was also prepared as the reference. **Fig. 4** shows the Schema of the four types of devices, and each type employed the PCBM layer with gradient thickness to find the optimal performance.

Before preparing the devices, all the thickness of the PCBM mentioned in the following was calibrated by an ellipsometer on the same standard planar glass substrates.

Table 1 Photovoltaic performances of the hybrid perovskite solar cells

Structure	PCBM (nm) spin-coating	PCBM (nm) Vaporing	J_{sc} (mA/cm^2) (ave±s.d.)	V_{oc} (V) (ave±s.d.)	FF (ave±s.d.)	PCE(%) (ave±s.d.)
DEVICE B ITO/PEDOT/$MAPbI_3$(two-step) /PCBM(spin-coating)/Ag	**60**	-	16.29±0.64	0.87±0.04	0.57±0.04	8.11±0.81
	80	-	15.91±0.59	0.88±0.05	0.58±0.03	8.10±0.78
	100	-	15.17±1.92	0.85±0.06	0.55±0.05	7.09±1.27
	120	-	14.06±1.11	0.86±0.05	0.51±0.04	6.15±1.03
DEVICE C ITO/PEDOT/$MAPbI_3$(two-step) /PCBM(Vapor deposition)/Ag	-	60	14.26±1.59	0.89±0.05	0.45±0.03	5.71±1.14
	-	80	15.89±1.27	0.92±0.04	0.47±0.04	6.87±0.88
	-	**100**	16.66±0.97	0.94±0.04	0.49±0.05	7.61±0.92
	-	120	15.77±1.17	0.95±0.03	0.48±0.06	7.19±1.01
DEVICE D	60	10	17.01±0.53	0.97±0.03	0.64±0.02	10.05±0.86
ITO/PEDOT/$MAPbI_3$(two-step)	**60**	**30**	17.21±0.48	0.98±0.02	0.66±0.02	11.09±0.62
/PCBM(spin-coating)	60	50	16.45±0.44	0.99±0.02	0.63±0.03	10.02±0.71
/PCBM(Vapor deposition)/Ag	60	80	14.76±0.54	0.98±0.02	0.63±0.02	9.11±0.69

*(ave±s.d.): The average and standard deviation (s.d.) of the 30 cells for each structure.

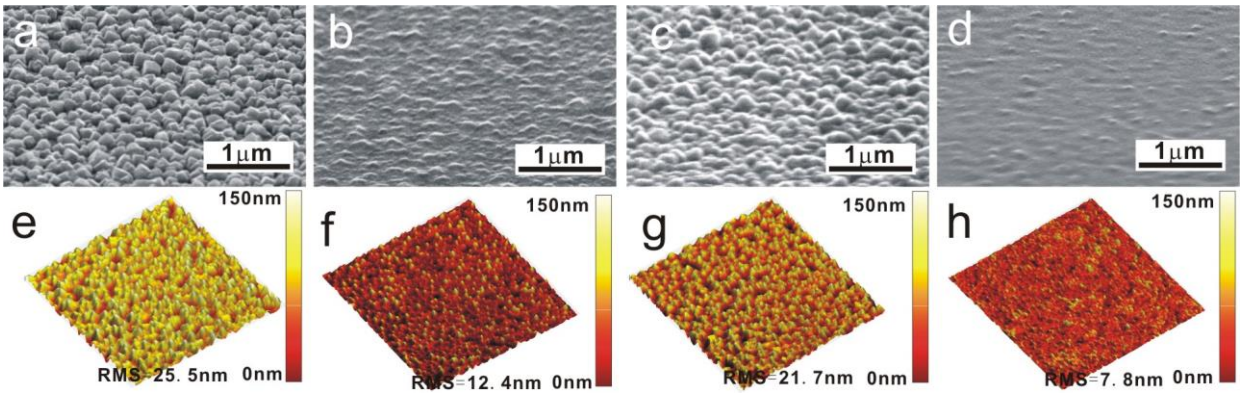

Fig. 5 tilt-angle SEM and 3-D AFM image of the $MAPbI_3$ layer (a and e), structure B: ITO/PEDOT/$MAPbI_3$(two-step)/PCBM(spin-coating) (b and f), structure C: ITO/PEDOT/$MAPbI_3$(two-step)/PCBM(Vaporing) (c and g) and structure D: ITO/PEDOT/$MAPbI_3$(two-step)/PCBM(spin-coating)/PCBM (Vaporing) (d and h).

To prove the repeatability of the devices, 30 cells of each structure were prepared. Performance of the devices were measured and shown in **Table.1.** As for the structure A based on one-step $MAPbI_3$ layer, it can be seen that structure A with 60 nm PCBM exhibits an average performance of PCE=7.37% (**Table.S1**). As the absence of material from some regions in the one-step $MAPbI_3$ film (pinholes) will result in direct contact of the ETL PCBM and the HTL PSS:PEDOT. This lead to a shunting path that is probably partially responsible for the lower FF and open-circuit voltage in the planar heterojunction devices.[25]

Two-step based $MAPbI_3$ layer could avoid the direct contact between HTL and ETL. Before preparing the structure B, C and D, the roughness of the two-step $MAPbI_3$ layer was observed for the more reasonable design of the devices. **Fig. 5**a and e show the tilt-angle SEM and 3-dimensional AFM image of the $MAPbI_3$ layer, and the root mean square (RMS) roughness is 25.5 nm. This rough surface requires a certain thickness of PCBM to completely fill in and smooth the $MAPbI_3$ layer.

We first tried the spin-coating only method of PCBM shown as structure B, and a series of various thickness (60~120nm) was prepared. It can be seen that devices with 60~80 nm PCBM exhibit a considerable 8.1% efficiency. This efficiency was comparable with the reported record. **Fig. 5**b and f show the tilt-angle SEM and 3-D AFM image of the structure B (PCBM=60nm) without Ag. We can see that the rough $MAPbI_3$ layer was relatively covered by the PCBM layer, and the RMS roughness was decreased obviously (RMS=12.4 nm). It is noted that the top of the $MAPbI_3$ crystals still can be observed in some regions, which lead to the direct contact between $MAPbI_3$ layer and Ag electrode when the real cell operated. This problem maybe limited the possibility of the higher performance. When the thickness was over 100 nm, the PCE obviously decreased, which was mainly due to the low film-forming quality of the excessive thickness. **Fig. S**1shows the tilt-angle SEM image of the structure B (PCBM=100 nm) without Ag. It was found that the surface changed irregular and rough, and the consequent poor interface would influenced the charge-transporting. The study of the structure B clarified that the only spin-coating process could not provide a suitable PCBM film for achieving a high efficient device.

Vapor deposition was another practical method to obtain a continuous and thickness-tunable film, and devices based on the only vapor deposition ETL method was shown as structure C, Result in **table 1** shows that with a 100 nm thickness of PCBM, an average of 7.61% efficiency of the devices was obtained. As we know that, films via vapor deposition process just inherited the morphology of the under-layer materials, thus it could hardly buffer the morphology of the architecture. **Fig. 5**c and g show the tilt-angle SEM and 3-D AFM image of the structure C (PCBM=100 nm) without Ag. It was found that though the $MAPbI_3$ layer was almost covered by the PCBM, the surface was still rough with a 21.7 nm RMS roughness. Such an asperous and inhomogeneous ETL would adverse to the fluent charge-transporting at the interface, and the relative low FF of the devices was the direct reflection. Study of the structure C indicated that a PCBM layer with enough thickness can be obtained by vapor deposition, but the roughness of the whole device was hardly decreased.

Based on the structure B and C, we designed the structure D for exploring the best performance. 60 nm PCBM was first deposited by spin-coating for initial filling, then a tunable PCBM layer was prepared by vapor deposition for further smoothing the interface and isolating the under-$MAPbI_3$ layer and metal electrode. Considering the the excessive thick PCBM could decrease the conductivity of the film, the range of the vaporing layer is located to 10~80 nm. A surprised efficiency with average of 11.09% appeared at the typical structure (ETL: 60nm + 30nm). **Fig. 5**d and h show the tilt-angle SEM and 3-D AFM image of the structure D (ETL: 60nm + 30nm) without Ag. We can see that this double-layer deposition process could efficiently cover the $MAPbI_3$ layer and obviously decrease the roughness. The rather small RMS roughness (7.8 nm) shows a nearly flat surface of the structure, which is the base of the planar inverted PCBM-$MAPbI_3$ solar cell. The good performance of the V_{oc}, FF and J_{sc} all clarified that strongly light-harvesting as well as good charge-transport were achieved. As the thickness of the PCBM film by vaporing increased, the performance of the device decreased which was mainly attributed to the low conductivity of the excessively thick PCBM layer.

As a response to the charge transport/recombination to some extent, dark-current was studied to further investigate the performance of different devices. **Fig. 6**a shows the average J–V characteristics of the devices based on structure B (ETL 60 nm), C (ETL 100 nm), and D (ETL 60+30 nm) under illumination and in the dark. The results show that the device D has the lowest

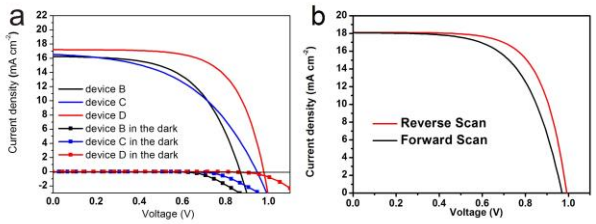

Fig. 6 (a) J-V characteristic of the device B, C and D under illumination and in the dark. (b) J-V characteristic of the device D with th highest efficiency

dark-current, which demonstrated the good performance on reducing the charge recombination loss and benefiting the charge transport. Larger dark-current value of device B and D was explained as follows: as for the device B, the bare protuberance of the $MAPbI_3$ layer (shown in **Fig. 4**a) in some region would directly contact with the Ag electrode, which lead to the interface recombination and reflected as the low FF and open-voltage. When coming to the device C, the film-forming property of the PCBM layer was poor and and surface was rough, and it reduced the fluency and uniformity of the charge-transporting at the $MAPbI_3$/ETL/Ag interface. The low FF of the device partially responded the disadvantages.

The highest performance of the device D was shown in **Fig. 6**b, exhibiting a performance of V_{oc}=0.99 V, J_{sc}=18.11 mA/cm^2, FF=0.68 and PCE=12.2% under reverse scaning, and V_{oc}=0.97 V, J_{sc}=18.09 mA/cm^2, FF=0.63 and PCE=11.04% under forward scaning. The hysteresis between forward and reverse J–V scan is the manifestation of a slow response time of the cell to a change in load.[26] The relative standard deviations of the parameters was less 10% (**shown in Table 1 and Fig. S**2), which indicated that the performance of the device was highly reproducible with low variation. The integrated current density derived from the EQE spectra in **Fig. S3** was in close agreement with the value measured under simulated sunlight shown in **Fig. 6**b. **Fig.S**4 shows a cross section SEM image of the inverse device D. The cross section SEM image also depicts a uniform deposition along the length of the device. Finally, the evolution of the PCE about the best device D was observed and shown in **Fig. S5**, which indicated a considerable stability.

Conclusions

In summary, we have developed a sequential layer-by-layer PCBM deposition method to fabricate planar perovskite solar cells. The solution/vapor process of the ETL could effectively fill in and smooth the rough $MAPbI_3$ layer. The cube-like and homogeneous $MAPbI_3$ layer promised the strong light-harvesting and benefited the charge transport. Meanwhile, planar and continuous PCBM film could separate the $MAPbI_3$ layer and Ag electrode for reducing recombination loss. With a rather low variation，the best PCE present a 12.2% efficiency, which was much higher than the reported PCBM-$MAPbI_3$ solar cells with the same structure. We hope that the integration of a simplified design, easy-fabrication, low-temperature, high-repeatability and considerable efficiency could provide a particular method to promote the development of the perovskite solar cells.

This work was financially supported by Basic Research Program of China (2013CB328705), National Natural Science Foundation of China (Grant Nos. 61275034), Ph.D. Programs Foundation of Ministry of Education of China (Grant No. 20130201110065).

Notes and references

*[a] Key Laboratory of Photonics Technology for information, Key Jiaotong University, Xi'an 710049, P. R. China
Tel: +86-29-82664867
E-mail: zhaoxinwu@mail.xjtu.edu.cn
*[b] State Key Laboratory for Mesoscopic Physics and Department of Physics,Peking University, Beijing 100871, PR China.
E-mail: lxxiao@pku.edu.cn
[#] These authors contributed equally to this work.

1. A. Kojima, K. Teshima, Y. Shirai and T. Miyasaka, *J. Am. Chem. Soc.*, 2009, 131, 6050.
2. J. Burschka, N. Pellet, S. J. Moon, R. Humphry-Baker, P. Gao, M. K. Nazeeruddin and M. Gratzel, *Nature*, 2013, 499, 316.
3. M. Z. Liu, M. B. Johnston and H. J. Snaith, *Nature*, 2013, 501.
4. O. Malinkiewicz, A. Yella, Y. H. Lee, G. M. Espallargas, M. Graetzel, M. K. Nazeeruddin and H. J. Bolink, *Nature Photonics*, 2014, 8, 128.
5. H. P. Zhou, Q. Chen, G. Li, S. Luo, T. B. Song, H. S. Duan, Z. R. Hong, J. B. You, Y. S. Liu and Y. Yang, *Science*, 2014, 345.
6. S. D. Stranks, G. E. Eperon, G. Grancini, C. Menelaou, M. J. P. Alcocer, T. Leijtens, L. M. Herz, A. Petrozza and H. J. Snaith, *Science*, 2013, 342.
7. G. C. Xing, N. Mathews, S. Y. Sun, S. S. Lim, Y. M. Lam, M. Gratzel, S. Mhaisalkar and T. C. Sum, *Science*, 2013, 342, 344.
8. S. Y. Sun, T. Salim, N. Mathews, M. Duchamp, C. Boothroyd, G. C. Xing, T. C. Sum and Y. M. Lam, *Energy & Environmental Science*, 2014, 7, 399.
9. D. Bryant, P. Greenwood, J. Troughton, M. Wijdekop, M. Carnie, M. Davies, K. Wojciechowski, H. J. Snaith, T. Watson and D. Worsley, *Adv. Mater.*, 2014, 26, 7499.
10. M. D. McGehee, *Nature*, 2013, 501, 323.
11. S. Kazim, M. K. Nazeeruddin, M. Gratzel and S. Ahmad, *Angew. Chem. Int. Edit.*, 2014, 53, 2812.
12. Y. Z. Ma, L. L. Zheng, Y. H. Chung, S. S. Chu, L. X. Xiao, Z. J. Chen, S. F. Wang, B. Qu, Q. H. Gong, Z. X. Wu and X. Hou, *Chem. Commun.*, 2014, 50, 12458.
13. J. Y. Jeng, Y. F. Chiang, M. H. Lee, S. R. Peng, T. F. Guo, P. Chen and T. C. Wen, *Adv. Mater.*, 2013, 25, 3727.
14. G. E. Eperon, V. M. Burlakov, P. Docampo, A. Goriely and H. J. Snaith, *Adv. Funct. Mater.*, 2014, 24, 151.
15. J. B. You, Z. R. Hong, Y. Yang, Q. Chen, M. Cai, T. B. Song, C. C. Chen, S. R. Lu, Y. S. Liu, H. P. Zhou and Y. Yang, *Acs Nano*, 2014, 8, 1674.
16. B. Conings, L. Baeten, C. De Dobbelaere, J. D'Haen, J. Manca and H. G. Boyen, *Adv. Mater.*, 2014, 26, 2041.
17. P. W. Liang, C. Y. Liao, C. C. Chueh, F. Zuo, S. T. Williams, X. K. Xin, J. J. Lin and A. K. Y. Jen, *Adv. Mater.*, 2014, 26, 3748.
18. H. B. Kim, H. Choi, J. Jeong, S. Kim, B. Walker, S. Song and J. Y. Kim, *Nanoscale*, 2014, 6, 6679.
19. C. W. Chen, H. W. Kang, S. Y. Hsiao, P. F. Yang, K. M. Chiang and H. W. Lin, *Adv. Mater.*, 2014, 26, 6647.
20. L. L. Zheng, Y. Z. Ma, S. S. Chu, S. F. Wang, B. Qu, L. X. Xiao, Z. J. Chen, Q. H. Gong, Z. X. Wu and X. Hou, *Nanoscale*, 2014, 6, 8171.
21. L. Hu, J. Peng, W. W. Wang, Z. Xia, J. Y. Yuan, J. L. Lu, X. D. Huang, W. L. Ma, H. B. Song, W. Chen, Y. B. Cheng and J. Tang, *Acs Photonics*, 2014, 1, 547.
22. Z. L. Zhu, Y. Bai, T. Zhang, Z. K. Liu, X. Long, Z. H. Wei, Z. L. Wang, L. X. Zhang, J. N. Wang, F. Yan and S. H. Yang, *Angew. Chem. Int. Edit.*, 2014, 53, 12571.
23. P. Docampo, J. M. Ball, M. Darwich, G. E. Eperon and H. J. Snaith, *Nature Communications*, 2013, 4.
24. D. Y. Liu and T. L. Kelly, *Nature Photonics*, 2014, 8, 133.
25. Q. Wang, Y. C. Shao, Q. F. Dong, Z. G. Xiao, Y. B. Yuan and J. S. Huang, *Energy & Environmental Science*, 2014, 7, 2359.
26. H. J. Snaith, A. Abate, J. M. Ball, *Journal of Physical Chemistry Letters*, 2014, 5, 1511.